Special Issue
Frontier in Characterization of Materials and Processes for Steel Manufacturing

ISIJ International, Vol. 62 (2022), No. 5, pp. 875–882
https://doi.org/10.2355/isijinternational.ISIJINT-2021-417

Sulfur Detection in Coke by Laser-Induced Breakdown Spectroscopy

Peng CHEN,[1)] Han LUO,[1)] Minchao CUI,[2,3)] Zhenzhen WANG,[1,2)]* Yoshihiro DEGUCHI[1,2)] and Junjie YAN[1,2)]

1) State Key Laboratory of Multiphase Flow in Power Engineering, Xi'an Jiaotong University, No. 28, Xianning West Road, Xi'an, 710049 China.
2) Graduate School of Advanced Technology and Science, Tokushima University, 2-1, Minamijyosanjima, Tokushima, 770-8506 Japan.
3) Key Laboratory of High Performance Manufacturing for Aero Engine (MIIT), Northwestern Polytechnical University, 127 West Youyi Road, Xi'an, 710072 China.

(*Received on September 1, 2021; accepted on November 4, 2021*)

Accurate determination of sulfur (S) content in coke is of great significance to improve the quality of iron and steel. In this study, the sulfur in coke standard samples was detected in argon (Ar) atmosphere using laser-induced breakdown spectroscopy (LIBS), and S I 182.034 nm was chosen as the analytical line. The experimental results showed that it was advantageous to detect S in the early stage of plasma generation. Compared with tablet samples, the spectral intensities of binder samples on the copper foil tape were greater and the signal-to-noise ratio (SNR) was also greater. As for reduplicate experiments, the coefficient of variation (CV) of spectral intensities of binder samples was 10.58% and that of tablet samples was 88.54%. The plasma signal induced by binder samples was stronger and more stable. The internal standard method and support vector machine regression (SVR) were used to quantitatively analyze the sulfur content in binder samples, and SVR showed more accurate prediction accuracy. R^2 of SVR with electron density and self-absorption correction was 0.965, root mean square error of prediction (RMSEP) was 0.18 wt.% and the limit of detection (LOD) was 0.026%. This result proved the applicability of binder for sulfur measurement in coke using LIBS.

KEY WORDS: laser-induced breakdown spectroscopy; coke; sulfur detection.

1. Introduction

Coke is the essential reagent in blast furnace (BF) ironmaking and the most important function of coke is to provide a channel for gas flow upward of carbon monoxide gas.[1)] The sulfur (S) content in coke is an indicator for its technological applications.[2)] Sulfur is one of the harmful impurities in the smelting process of pig iron, which reduces the quality of pig iron. If the sulfur content is greater than 0.07%, pig iron becomes waste. It is necessary to detect the sulfur in coke in real-time because coke is the main source of sulfur in charge. The conventional analytical techniques for the sulfur content include the high temperature combustion method,[3)] X-ray fluorescence spectrometry (XRF),[4)] and so on.[5)] It takes much time to detect sulfur using the high-temperature combustion method and it does not meet the needs of real-time detection. As for XRF, the sample preparation process is complex. As an emission spectroscopy technology, due to the advantages of multi-element analysis and rapid measurement, laser-induced breakdown spectroscopy (LIBS) has been proved to be an effective detection technology for monitoring of steel manufacture process[6,7)] and measurement of coal, petroleum coke, and other fuels.[8–13)]

Scholars have researched sulfur detection using LIBS. Ruan *et al.*[14)] detected the spectra of alloy steel in the range of 200–800 nm. Due to the characteristics of low sulfur content and difficult excitation of sulfur spectra, only two weak sulfur lines of S II 543.2 nm and S II 543.3 nm were identified. Hrdlička *et al.*[15)] detected sulfur in concrete in an atmosphere of 600 mbar helium. S I 921.29 nm was chosen as the analytical line and the limit of sulfur detection was ensured to be 0.0025%. Gazeli *et al.*[16)] detected sulfur in organic soil samples using LIBS in the vacuum ultraviolet (VUV) spectral region. S I 921.3 nm was disturbed by O I 926.6 nm and S I 182.1 nm was more appropriate to be chosen as the analytical line. The above analysis showed that LIBS had great potential to be applied to the measurement of sulfur in solid samples. For the demand for online detection, it is necessary to research the detection of sulfur

* Corresponding author: E-mail: zhenzhen-wang@xjtu.edu.cn

content in open space.

Coke often appeared in the form of powder in the industry. The signal of laser-induced powder plasma is weak. Scholars tried to improve signal stability using tablet pressing, adhesive bonding, flow, *etc.* Stehrer *et al.*[17] reported on laser ablation and optical plasma emission spectroscopy of loose iron oxide (Fe_2O_3) nano-particle powder without any pre-treatment and fixation of the powder. For the loose powder and the pressed powder pellets, they showed similar plasma states. Whereas craters with a few millimeters in diameter and depth were formed at the focus, the powder surface needed to be continuously smoothed. Feng *et al.*[18] pressed standard powdery bituminous coal samples with the pressure of 20 tons. They found that the evaporated volatiles might react with air to produce a flame. And then it affected the plasma spectra. For some samples, it is difficult to obtain a pressed pellet that could sustain multiple laser shots. Ctvrtnickova *et al.*[9] measured the carbon content in fly ash by mixing the binder with the fly ash. They found that when adding 80 wt.% KBr into the fly ash, the prediction results of carbon content were the best. Wildly used adhesives including sucrose, starch, $Ca(OH)_2$, epoxy resin glue, water glass (Na_2SiO_3), *etc.*[19–22] As tablet pressing was required after adding adhesive to samples, pressure and other factors would still affect LIBS test results. Thus, it was necessary to consider the possibility of obtaining a solid surface only by adding adhesive.

In this work, two kinds of sample pretreatment methods were adopted, respectively. As for binder samples, the coke was bonded with the water glass on copper foil tape without compression. As for tablet samples, the coke was pressed without adding adhesive. The plasma signals of binder samples and tablet samples with different delay times and pulse number were compared. Based on the spectral intensities, signal-to-noise ratio (SNR), stability, an appropriate sample preparation method was chosen for the establishment of the calibration model. Besides, considering the matrix effect, the internal standard method and support vector machine regression (SVR) were used to improve the accuracy of the model in predicting sulfur content.

2. Experimental Setups

A schematic diagram of the experimental setup is depicted in **Fig. 1**. This setup consisted mainly of the optical path and the gas path. A Q-switched pulsed Nd: YAG laser (Hamamatsu Photonics Co., Ltd., L12968-01) was operated at a pulse width of about 10 ns and an output wavelength of 1 064 nm. The laser of a repetition rate of 10 Hz was applied with a laser power of 10 mJ. The pulse laser irradiated directly on the sample to induce plasma through reflection mirrors, a filter (cutoff wavelength = 200 nm) and lens (f = 40 mm). The chamber was purged with Ar flow at a speed of 30 L/min and its volume was about 1 L. Then, the plasma emission was collected to the UV coat optical fiber (Mitsubishi Cable Industries LTD., DUV-190-1). Next, the spectrometer (SOL, NP-250-2M) recorded the optical signal with the center wavelength of 180 nm at a resolution of 0.012 nm/pixel, and the center wavelength of 200 nm at a resolution of 0.076 nm/pixel simultaneously. The monochromatic light was passed into the ICCD camera (Andor, iStar DH334T-18U-03) for the photoelectric conversion. The trigger timing of the laser and the ICCD camera was controlled by a delay generator (Stanford Research Systems, Model DG645). To obtain a strong spectral signal, the gate width was set to 100 μs, the exposure time was set to 5.05 s, and the delay time was set to 1, 10, 20, 50, and 100 ns respectively.

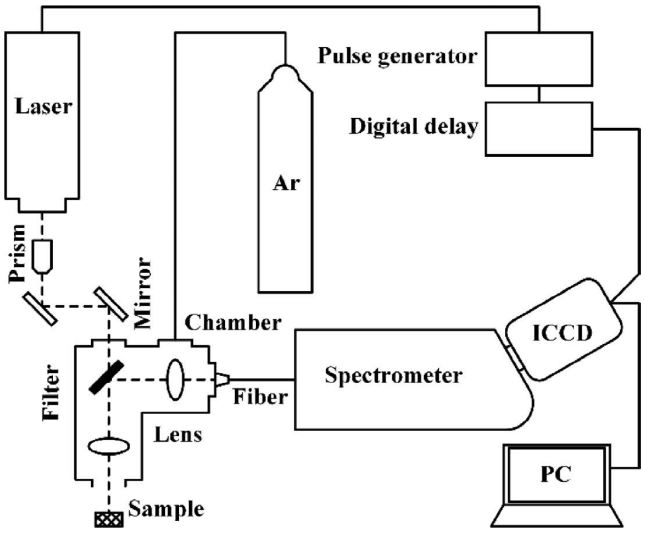

Fig. 1. Schematic diagram of LIBS experimental system.

Table 1. Composition of the standard coke samples.

No.	Sample	Content (wt.%)			
		S	Ash	Volatiles	C
1	GBW(E)110057	0.53	11.15	2.37	85.94
2	GBW(E)110011b	0.64	13.06	1.30	84.97
3	GBW(E)110011d	0.68	12.85	1.32	85.13
4	GBW(E)110012d	0.77	14.05	1.48	83.67
5	GBW(E)110062	0.89	15.05	1.42	82.62
6	GBW(E)110063	1.04	17.00	1.44	80.50
7	ZBM129A	1.22	14.40	1.66	82.69
8	GBW(E)110015	1.33	17.15	3.27	78.23
9	GBW(E)110060	1.42	21.04	1.49	76.03
10	ZBM143	2.10	17.40	1.85	78.64
11	ZBM145	2.60	19.26	1.76	76.36

The standard coke samples were provided by Jinan Zhongbiao Science and Technology Co., Ltd., and the chemical composition of the standard coke samples was shown in **Table 1**. The sulfur content of the coke samples was evaluated by the Eschka method. Each coke sample was screened by 0.18 mm to ensure uniformity. To improve the measurement repeatability, powder pellets preparation and binder preparation were utilized, respectively, to help anthracite samples to form a smooth surface strong enough to sustain multiple laser shots. As for binder sampling, each coke sample was mixed with Na_2SiO_3. The weight percentage of Na_2SiO_3 of each sample was 50 wt.%. The samples were brushed evenly on the copper foil tape to form binder samples and they completely solidified after being set for 4 hours. As for tablet sampling preparation, 0.6 g of coal

was introduced into a manual press where it underwent the pressure of 1 t during 5 min.

3. Results and Discussion

To improve analysis accuracy of S content in coke, sample preparation methods and calibration models were studied. As for sample preparation methods, plasma signals induced by binder samples and tablet samples were compared. As for quantitative models, calibration accuracy of the internal standard method and SVR were compared.

3.1. Comparison of the Tablet and Binder Samples

As for LIBS measurement, delay time was an important parameter in element detection.[23] It was necessary to study the signal characteristics of binder samples and tablet samples in different delay times. The stability of LIBS signals needed test under one optimal delay time. In addition, the correlation between S content and S spectral intensities was observed for a preliminary quantitative analysis. According to the signal characteristics and preliminary calibration accuracy, appropriate sample preparation method would be selected.

3.1.1. Influence of the Delay Time

The emission intensity of plasma at the early stage of generation was high. As the plasma cooled, the emission became weaker.[23] It is necessary to exam LIBS spectra in the early stage of plasma generation.

To clearly observe the sulfur spectrum, sample No. 11 with the highest sulfur content was selected for detection. **Figure 2** showed the spectra in the wavelength range of 180.5–186.5 nm of sample No. 11 in the delay time of 1, 10, 20, 50, and 100 ns. The mean measurement results of three laser pulses were offered. The spectra were normalized by the max intensity of the whole data. According to the NIST database,[24] the information of spectral lines was checked and shown in **Table 2**. S I 180.731 nm, S I 182.034 nm, and S I 182.624 nm could be observed clearly in the Ar atmosphere. Continuous background radiation was dominant in the early stage of plasma generation and it was easy to cause interference to the desired signal. Background intensities varied with the delay time in Fig. 2, which meant that the delay time would have a significant impact on the spectra measurement. In this study, the standard deviation of noise around adjacent spectral peaks was adopted to evaluate SNR. **Table 3** listed the intensities and SNR of the S spectral lines of the tablet samples in different delay times. Compared with those of S I 180.731 nm and S I 182.624 nm, the intensities and SNR of S I 182.034 nm were the highest. The higher intensities and SNR meant higher detection sensitivity. Therefore, S I 182.034 nm was chosen as the analytical spectral line.

Figure 3 showed intensities and SNR of S I 182.034 nm in different delay times. Error bars were composed of three

Table 2. The spectral information of coke.

Wavelength (nm)	E_i (cm^{-1})	E_k (cm^{-1})
S I 180.731	0	55 330.81
S I 182.034	396.06	55 330.81
S I 182.624	573.64	55 330.81
Ca II 183.801	13 650.19	68 056.91
Ca II 184.006	13 710.88	68 056.91
Si I 184.747	77.12	54 205.09
Si I 185.067	223.16	54 257.58
Al II 185.803	37 453.91	91 274.50
Al II 186.231	37 577.79	91 274.50
C I 193.090	10 192.66	61 981.83

Table 3. The intensities and SNR of the S spectral lines of the tablet samples in different delay times.

Item	Line (nm)	Delay time (ns)				
		1	10	20	50	100
Intensities (arb. unit)	S I 180.731	0.62	0.63	0.51	0.50	0.46
	S I 182.034	0.93	1.00	0.76	0.78	0.69
	S I 182.624	0.54	0.54	0.45	0.44	0.39
SNR (-)	S I 180.731	53	39	45	43	44
	S I 182.034	85	67	79	88	73
	S I 182.624	40	38	46	41	43

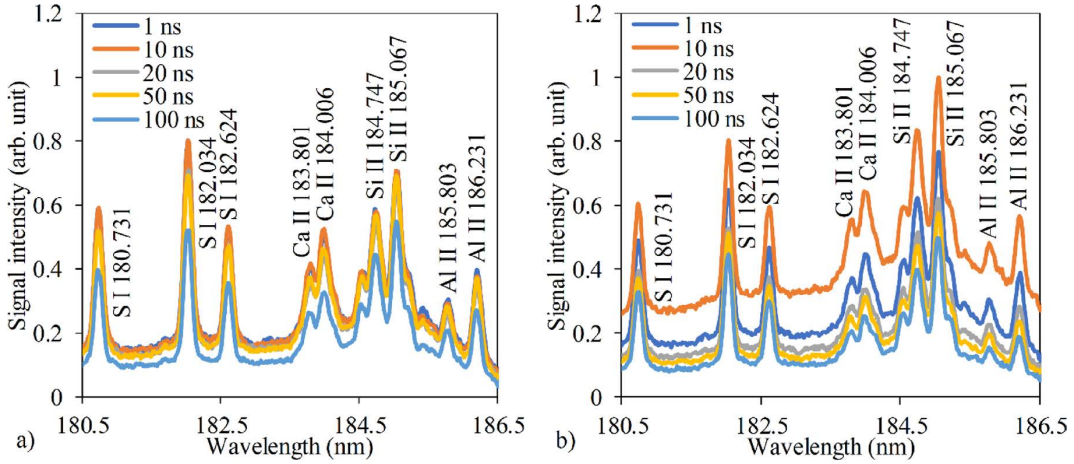

Fig. 2. Measured spectra of sample No. 11 in different delay times. (a) Measured spectra of the binder sample. (b) Measured spectra of the tablet sample. (Online version in color.)

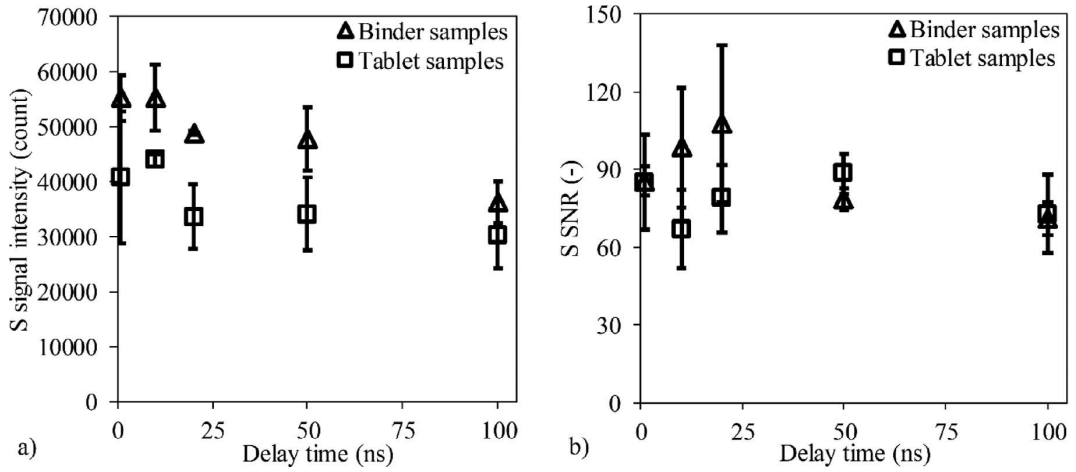

Fig. 3. Delay time dependence of S measurement results for sample No. 11. (a) Intensities of S I 182.034 nm in different delay times. (b) SNR of S I 182.034 nm in different delay times.

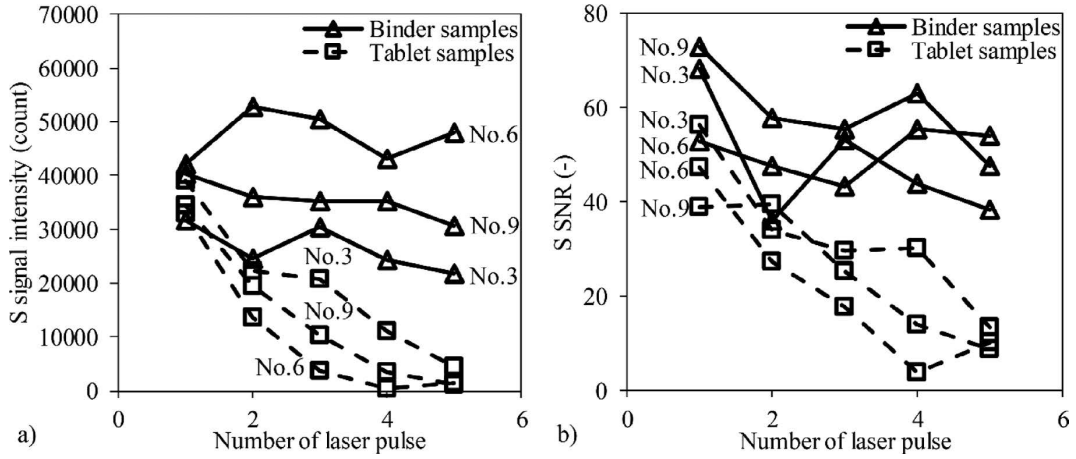

Fig. 4. Measured results at different laser pulse numbers for samples No. 3, 6, and 9. (a) Intensities of S I 182.034 nm. (b) SNR of S I 182.034 nm.

measurements. The intensities of S I 182.034 nm increased slightly and reached their maximum in the delay time of 10 ns. Then they gradually decreased after 10 ns. It was easy to understand that the plasma was gradually cooled by the surrounding cold mixed gas, and the emission intensities of the spectra gradually decreased with the increase of delay time. This trend that firstly increased and then decreased accorded with the trend of plasma temperature change.[25] The signal intensities of the binder sample were higher than those of the tablet sample. For tablet samples, the surface would be easily stratified during the LIBS measurement process when the laser pulse shot its surface. The local density of the loose surface was lower, resulting in less laser ablation and lower spectral intensities. SNR of the binder samples reached its maximum in the delay time of 20 ns. In the initial stage of laser plasma formation, the violent collision between electrons, excited ions and atoms could produce strong continuous background spectra. The atomic spectra were superimposed on the continuous background spectra. Because the attenuation of the atomic spectra was slower than that of the continuous background spectra,[26] the maximum SNR appeared later than the maximum intensity. As the plasma declined, instrument noise and environmental background noise would occupy a dominant position. Higher SNR meant a better detection limit. It illustrated that when the measurement delay time was small, binder preparation was beneficial to signal detection.

3.1.2. Influence of Pulse Number

Different kinds of coke samples were measured in the delay time of 10 ns. The mean measurement results of five laser pulses were offered. Measured results of S I 182.034 nm of different pulse numbers for samples No. 3, 6, and 9 were shown in **Fig. 4**. In general, the intensities and SNR of the binder samples were greater than those of the tablet samples. With the increase of laser pulse numbers, the spectral intensities of the tablet samples gradually decreased and the spectral intensities of the binder samples remained relatively stable. There would be stratified surface near the laser focusing position because of the strong shock wave press and the incompact surface of the tablet samples. With the increase of laser pulse numbers, the phenomenon of surface stratification was intensified, which led to less sample ablation and lower intensities of spectral signals. Because the binder samples surface was compact, multiple pulses would not cause surface stratification. Therefore, the signal intensities of the binder samples would not decrease greatly. In sum, the reason for the low stability of repeated experiments was that the compactness of the tablet samples was low, which led to a different ablation amount of the samples

in multiple experiments. However, as for the measurement result of the 5th pulse of the tablet sample, SNR was still valid, which reached about 8.

On the contrary, the intensities of the binder sample No. 6 increased slightly with the increase of pulse numbers. The surface of the binder samples was compact and there would be a small crater near the laser focusing position. The evaporated material in the crater could effectively absorb the subsequent laser pulse energy under the constraint of aperture, further ionize, and absorb the laser energy through inverse bremsstrahlung.[27] The coefficient of variation (CV) of the binder samples of No. 3, 6, and 9 was 10.58% and that of the tablet samples was 88.54%. Repeated measurement stability of the binder samples was higher than that of the tablet samples.

3.1.3. Influence of Coke Types

Considering the high dispersion degree of the repeated results, the first three experimental results were discussed in this chapter. According to the Scheibe-Lomakin formula (S-L):

$$I = am^n \quad \text{..... (1)}$$

where I is the spectral line intensity, a is a constant related to the measurement condition and atomic information of the spectral line, m is the content of the measured particle, and n is the self-absorption parameter. When the particle content is low, n was equal to 1. **Figure 5** showed the intensities of S I 182.034 nm of the samples No. 1–10. The fitting curve between dependent variables and independent variables was called the calibration curve. R^2 of the intensities and the content was 0.19 for the binder samples, which indicated a low correlation. The intensities of S did not increase with the increase of the S content like Formula 1. The poor outcome would be explained by the matrix effect. For different samples, the excitation degree of laser-induced plasma varied with the matrix. The results of the tablet samples were more discrete than those of the binder samples from the error bar. It was similar to the conclusion in the preceding chapter.

To improve the results given by the S-L method, the spectral data were normalized by the intensity of the main element.[28] The formula of the internal standard method is:

$$\frac{I_t}{I_r} = \frac{a_t m_t}{a_r m_r} = a_0 m_t \quad \text{..... (2)}$$

where t is the target element, r is the internal standard element. It could be seen that the C content was the highest proportion of the total content from Table 1. The C content was relatively stable and C was chosen as the internal standard element. The analysis results of the internal standard method were given in **Fig. 6**. The model output of Figs. 6(a), 6(b) was the content ratio of S and C. The model output of Figs. 6(c), 6(d) was the content of S. R^2 of the two groups was similar, which showed that it was feasible to simplify the output to the content of S. R^2 of the calibration curve of the binder samples was 0.755 and that of the tablet samples increased from 0.0688 to 0.629. Similarly, the discreteness of the experimental results was significantly reduced. Compared with the unoptimized results, there was a significant improvement for both the binder samples and the tablet samples. This improvement might be attributed to the fact that the internal standard method could reduce the impact of laser energy, the inter-element effect, *etc.* In addition, the calibration results of the binder samples were better than those of the tablet samples. The limit of detection (LOD) could be calculated by the following expression:[29]

$$\mathrm{LOD(wt.\%)} = 3\sigma_\alpha / a \quad \text{..... (3)}$$

where σ_α is the standard deviation of the measurements for the samples with the five lowest element content.[30] LOD of the binder samples was 1.00 wt.% and that of the tablet samples was 0.90 wt.%. The calibration results of the binder samples were better than those of the tablet samples as determined by the internal standard method. However, the calibration results of the binder samples need further optimization to improve the fitting accuracy.

3.2. Quantitative Analysis of Sulfur in Coke

Support vector machine (SVM) is a kind of generalized linear classifier that classifies data by supervised learning.[31] Its decision boundary is the maximum margin hyperplane of learning samples. SVR can be obtained by extending SVM from classification problem to regression problem. SVR model could perform well in the relationship between LIBS spectra and the content, *etc.*[32–34] The basic ideas of SVR can

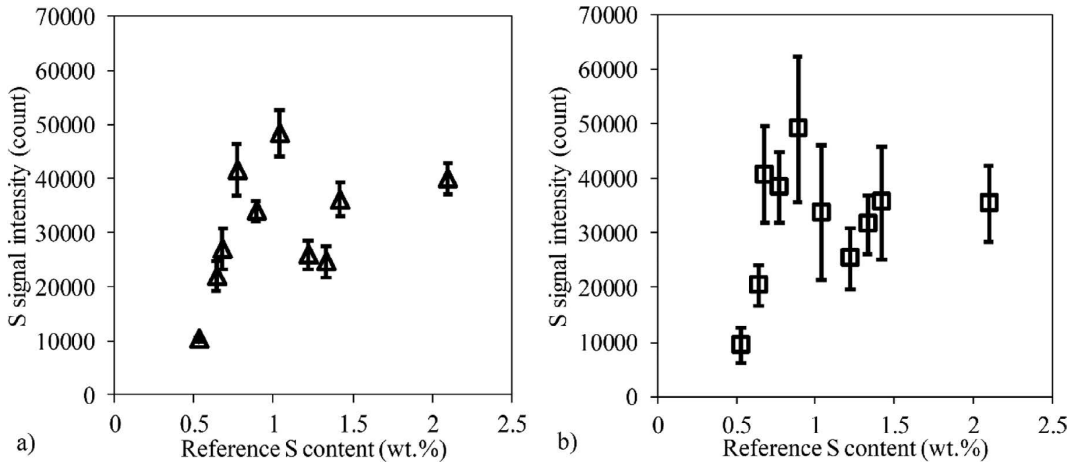

Fig. 5. The intensities of S I 182.034 nm of different samples. (a) The binder samples. (b) The tablet samples.

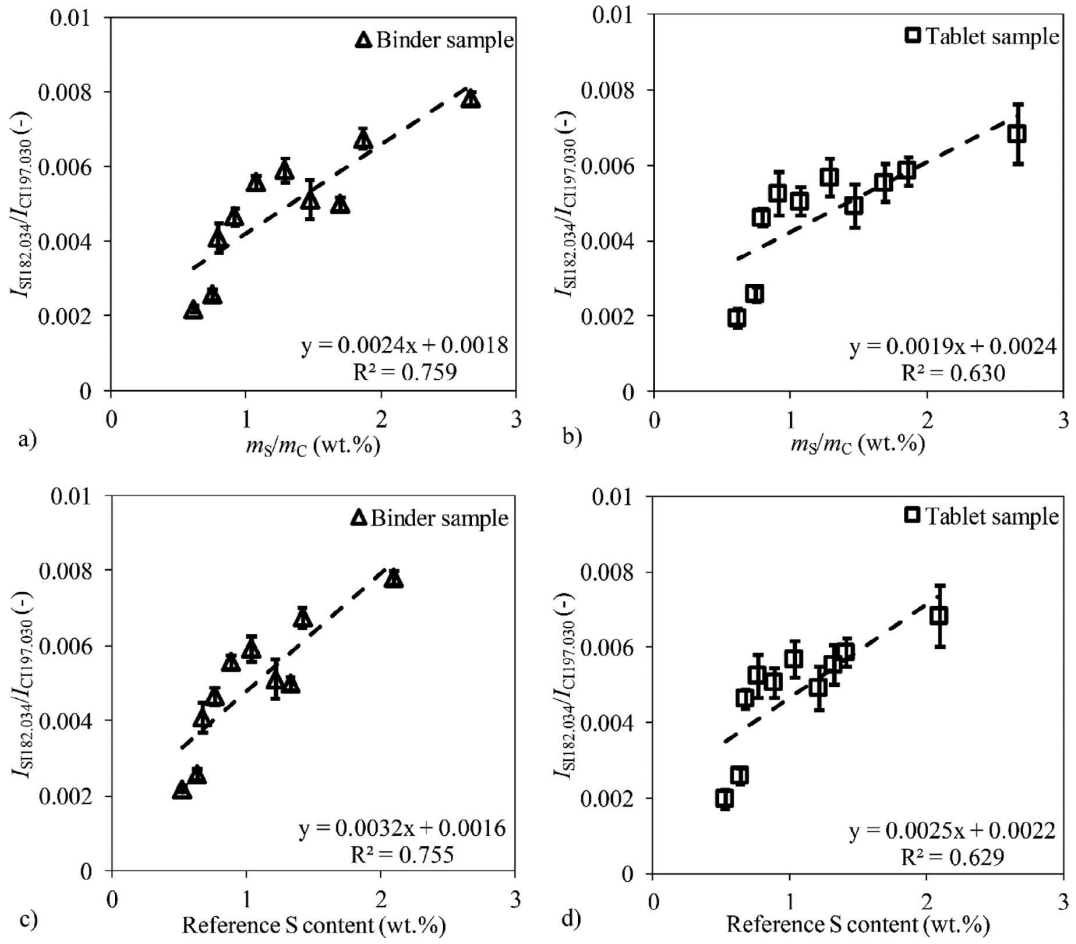

Fig. 6. The intensities of S I 182.034 nm of different samples by internal standard method. (a) Binder samples. Output: m_S/m_C. (b) Tablet samples. Output: m_S/m_C. (c) Binder samples. Output: m_S. (d) Tablet samples. Output: m_S.

be concluded in the following two steps: (i) the original data are first nonlinearly mapped into a high dimensional feature space, and then (ii) a linear function is fitted to approximate the latent function between input variables and output variables.[35] SVR can be transformed into a dual problem with constraint conditions:[36]

$$\min_{\omega} \frac{1}{2}|\omega|^2 + c\sum_{i=1}^{n}\xi_i + \xi_i^*, i = 1,2,\cdots,n$$
$$\text{s.t.}\begin{cases} y_i - \omega\cdot\phi(x) - b \le \varepsilon + \xi_i; \\ \omega\cdot\phi(x) + b - y_i \le \varepsilon + \xi_i^*; \\ \xi_i, \xi_i^* \ge 0. \end{cases} \quad \text{..... (4)}$$

where ω is the weight, c is the penalty factor, ξ is the relaxation factor, ε is the insensitive loss function, b is the threshold, and y is the output value. The above optimizing problem can be converted to be a minimization approximate function:

$$f(x) = \sum_{i=1}^{n_{SV}}(\alpha_i - \alpha_i^*)K(x_i, x) + b \quad \text{..... (5)}$$

where α is the Lagrange multiplier, n_{SV} is the number of support vectors, $K(x_i,x)$ is the kernel function and x was the input value. In this study, RBF was chosen as the kernel function:

$$K(x_i, x) = \exp(-g\|x - x_i\|^2) \quad \text{..... (6)}$$

where g is the constant of the kernel function. The relevant calculation was carried out by MATLAB R2020a and SVR was realized by the LIBSVM package.[37] Samples No. 3 and No. 8 were chosen as the test set and the others were chosen as the training set. To avoid under-fitting results, the grid search method was adopted to optimized c and g. ε was 0.01% and other parameters took default values. To avoid over-fitting results, 3-fold cross-validation was adopted to test the training results. According to the internal standard method, the input values of SVR were the intensities of C I 197.090 nm and S I 182.034 nm (*i.e.*, $I_{input} = [I_{CI197.090}, I_{SI182.034}]$), and the output values were the S content. The spectra were also affected by plasma state, self-absorption effect, *etc.*[38] Self-absorption could be indicated by the intensity ratio of spectral lines of the same element and the same ionization state. Hence, the lines intensity ratio of Si I 184.747 nm and Si I 185.067 nm (*i.e.*, $I_{SiI184.747}/I_{SiI185.067}$) was selected as the index to indicate self-absorption. The plasma broadening of laser-induced breakdown spectrum was mainly caused by electron collision, and the ion broadening could be ignored. Doppler broadening formula could be simplified as below:[39]

$$\Delta\lambda_{1/2} = 2\omega\left(\frac{n_e}{10^{16}}\right) \quad \text{..... (7)}$$

where $\Delta\lambda_{1/2}$ is FWHM, ω is the electron impact parameter, and n_e is the electron density. Because of the good linear relationship between FWHM and the electron density, and for simplified calculation, FWHM of S I 182.034 nm was

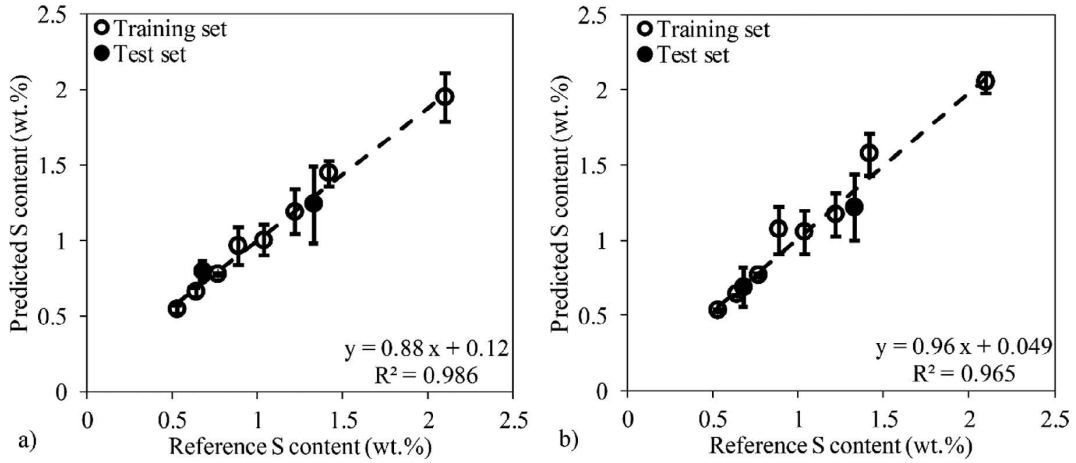

Fig. 7. Calibration plots generated by SVR of the S content using binder samples. (a) SVR without correction. (b) SVR with electron density and self-absorption correction.

selected to indicate the electron density. Sulfur intensity, carbon intensity, self-absorption index, and electron density index were taken as the input values of SVR (I_{input}' = [$I_{CI197.090}$, $I_{SI182.034}$, $I_{SiI184.747}/I_{SiI185.067}$, $\Delta\lambda_{1/2}$]). The regression plots generated by SVR using binder samples were shown in **Fig. 7** under the optimal *c* and *g*. There is a good agreement between the reference value and the predicted value of SVR. R^2, RMSE and LOD were taken as indexes to evaluate the fitting accuracy and prediction accuracy. They could be calculated as follows:

$$R^2 = 1 - \frac{\sum_{i=1}^{p}(\hat{y}_i - y_i)^2}{\sum_{i=1}^{p}(\bar{y}_i - y_i)^2} \quad \text{..... (8)}$$

$$RMSE = \sqrt{\frac{\sum_{i}^{p}(\hat{y}_i - y_i)^2}{p}} \quad \text{..... (9)}$$

where y is the reference value, $\bar{y}$ is the predicted value, $\hat{y}$ is the average of the predicted value and p is the number of measurements. R^2, root mean square error of prediction (RMSEP, results of the test set), and LOD of the internal standard method and SVR were listed in **Table 4** for binder samples. Machine learning algorithms such as SVR were prone to overfitting. This kind of method could get a good fitting result on the training data, but it could not fit the data well in the prediction set. To avoid it, the prediction accuracy such as RMSEP was more highly valued. R^2 of SVR was greater than 0.96, which was greater than that of the internal standard method, and it suggested that the fitting accuracy of SVR was better than that of the internal standard method; RMSEP of SVR was less than 0.2 and it was less than that of the internal standard method, which suggested that prediction accuracy of SVR was better than that of the internal standard method. As for LOD, that of SVR without correction was 0.081 wt.% and that of the internal standard method was 0.074 wt.%. Obviously, the introduction of the machine learning method reduced the stability of measurement results, and then reduced the reliability of results compared with the internal standard method. LOD of SVR with electron density and self-absorption correction was 0.026% and it was less than that of the internal standard method. The introduction of information about physical helped improve model stability. This improvement was attributed to the better robustness of the physical principle-based model over a wider range of sample matrixes.[40] In sum, the measurement accuracy could be improved by using SVR and the introduction of appropriate physical information was helpful to the robustness of the model.

Table 4. Performance of internal standard method and SVR for analysis of the S content.

Performance	R^2	RMSEP (wt.%)	LOD (wt.%)
Internal standard method	0.751	0.230	0.074
SVR without correction	0.986	0.199	0.081
SVR with correction	0.965	0.180	0.026

4. Conclusion

The feasibility of using binder for sulfur measurement in coke has been studied in this paper. The standard coke samples were pressed, and brushed evenly on the copper foil tape with binder, respectively. The LIBS experiments in detail were carried out in the ideal delay time of 10 ns. Intensities, SNR and stability of spectral signals induced from binder samples were greater than those of tablet samples. Using the internal standard method, R^2 of the quantitative model was 0.76 with binder samples, and that was 0.64 with tablet samples. These showed that binder samples were more suitable for measuring sulfur in coke compared with tablet samples.

The sulfur content in binder samples was quantitatively analyzed by SVR to improve measurement accuracy. R^2 was 0.986, RMSEP was 0.199 wt.%, and LOD was 0.081 wt.% of SVR without correction. R^2 was 0.965, RMSEP was 0.180 wt.%, and LOD was 0.026 wt.% of SVR with electron density and self-absorption correction. Compared with SVR without correction, SVR with electron density and self-absorption correction could improve the prediction accuracy of quantitative analysis. Therefore, binder samples on the copper foil tape were suitable for LIBS used for sul-

fur measurement in coke.

Acknowledgement

This work was supported by Young Talent Fund of University Association for Science and Technology in Shaanxi, China (No. 20190401) and National Natutal Science Foundation of China (No. 62005218).

REFERENCES

1) M. M. Sun, J. L. Zhang, K. J. Li, H. T. Li, Z. M. Wang and C. H. Jiang: *ISIJ Int.*, **60** (2020), 1918. https://doi.org/10.2355/isijinternational.ISIJINT-2020-079
2) R. Fernández-Ruiz, M. J. Redrejo, K. E. J. Friedrich, N. Rodríguez and R. Amils: *Spectrochim. Acta B*, **174** (2020), 105997. https://doi.org/10.1016/j.sab.2020.105997
3) ISO 351: 1996, Solid mineral fuels — Determination of total sulfur — High temperature combustion method.
4) T. Čechák and L. Thinová: *Radiat. Phys. Chem.*, **61** (2001), 759. https://doi.org/10.1016/S0969-806X(01)00397-8
5) Y. W. Ma, W. Zhang, Z. Xiong, H. H. Cui, Q. Z. Li, R. Zhou, Y. J. Zhang, X. Y. Li, X. Y. Zeng and Q. Li: *J. Anal. At. Spectrom.*, **35** (2020), 1458. https://doi.org/10.1039/C9JA00448C
6) Z. Z. Wang, Y. Deguchi, F. J. Shiou, J. J. Yan and J. P. Liu: *ISIJ Int.*, **56** (2016), 723. https://doi.org/10.2355/isijinternational.ISIJINT-2015-542
7) Z. Z. Wang, Y. Deguchi, F. J. Shiou, S. Tanaka, M. C. Cui, K. Rong and J. J. Yan: *ISIJ Int.*, **60** (2020), 971. https://doi.org/10.2355/isijinternational.ISIJINT-2019-317
8) X. J. Xu, A. Z. Li, X. S. Wang, C. J. Ding, S. L. Qiu, Y. G. He, T. Q. Lu, F. He, B. S. Zou and R. B. Liu: *J. Anal. At. Spectrom.*, **35** (2020), 984. https://doi.org/10.1039/C9JA00443B
9) T. Ctvrtnickova, M. P. Mateo, A. Yañez and G. Nicolas: *Spectrochim. Acta B*, **64** (2009), 1093. https://doi.org/10.1016/j.sab.2009.07.032
10) J. L. Tarazona, J. Guerrero, R. Cabanzo and E. Mejía-Ospino: *Appl. Opt.*, **51** (2012), B108. https://doi.org/10.1364/AO.51.00B108
11) W. H. Zhang, Z. Zhou, P. Lu, T. F. Sun, W. L. Sun and J. Q. Lu: *Spectrochim. Acta B*, **177** (2021), 106076. https://doi.org/10.1016/j.sab.2021.106076
12) S. M. Z. Iqbal, Z. Uddin, N. Ahmed, Z. A. Umar and M. A. Baig: *Laser Phys.*, **29** (2019), 036101. https://doi.org/10.1088/1555-6611/aaff58
13) H. M. Jun, J. H. Kim, S. H. Lee and J. J. Yoh: *Energy*, **160** (2018), 225. https://doi.org/10.1016/j.energy.2018.07.016
14) F. Q. Ruan, J. Qi, C. H. Yan, H. S. Tang, T. L. Zhang and H. Li: *J. Anal. At. Spectrom.*, **32** (2017), 2194. https://doi.org/10.1039/C7JA00231A
15) A. Hrdlička, J. Hegrová, K. Novotný, V. Kanický, D. Prochazka, J. Novotný, P. Modlitbová, L. Sládková, P. Pořízka and J. Kaiser: *Spectrochim. Acta B*, **142** (2018), 8. https://doi.org/10.1016/j.sab.2018.01.015
16) O. Gazeli, D. Stefas and S. Couris: *Materials*, **14** (2021), 541. https://doi.org/10.3390/ma14030541
17) T. Stehrer, B. Praher, R. Viskup, J. Jasik, H. Wolfmeir, E. Arenholz, J. Heitz and J. D. Pedarnig: *J. Anal. At. Spectrom.*, **24** (2009), 973. https://doi.org/10.1039/B817279J
18) J. Feng, Z. Wang, L. West, Z. Li and W. D. Ni: *Anal. Bioanal. Chem.*, **400** (2011), 3261. https://doi.org/10.1007/s00216-011-4865-y
19) M. Garcimuño, D. M. D. Pace and G. Bertuccelli: *Opt. Laser Technol.*, **47** (2013), 26. https://doi.org/10.1016/j.optlastec.2012.08.011
20) L. L. Shi, Q. Y. Lin and Y. X. Duan: *Talanta*, **144** (2015), 1370. https://doi.org/10.1016/j.talanta.2015.07.085
21) B. Lal, H. B. Zheng, F. Y. Yueh and J. P. Singh: *Appl. Opt.*, **43** (2004), 2792. https://doi.org/10.1364/AO.43.002792
22) T. B. Yuan, Z. Wang, L. Z. Li, Z. Y. Hou, Z. Li and W. D. Ni: *Appl. Opt.*, **51** (2012), B22. https://doi.org/10.1364/AO.51.000B22
23) L. Y. Yu, J. D. Lu, W. Chen, G. Wu, K. Shen and W. Feng: *Plasma Sci. Technol.*, **7** (2005), 3041. https://doi.org/10.1088/1009-0630/7/5/015
24) NIST: NIST Atomic Spectra Database Lines Form, https://physics.nist.gov/PhysRefData/ASD/lines_form.html, (accessed 2021-07-01).
25) M. C. Cui, Y. Deguchi, C. F. Yao, Z. Z. Wang, S. Tanaka and D. H. Zhang: *Spectrochim. Acta B*, **167** (2020), 105839. https://doi.org/10.1016/j.sab.2020.105839
26) S. Wu, T. L. Zhang, H. S. Tang, K. Wang, X. F. Yang and H. Li: *Anal. Methods*, **7** (2015), 2425. https://doi.org/10.1039/C4AY02601B
27) M. C. Cui, H. R. Guo, Y. D. Chi, L. Tan, C. F. Yao, D. H. Zhang and Y. Deguchi: *Spectrochim. Acta B*, **191** (2022), 106398. https://doi.org/10.1016/j.sab.2022.106398
28) P. Pořízka, J. Klus, E. Képeš, D. Prochazka, D. W. Hahn and J. Kaiser: *Spectrochim. Acta B*, **148** (2018), 65. https://doi.org/10.1016/j.sab.2018.05.030
29) M. Z. Martin, N. Labbé, N. André, S. D. Wullschleger, R. D. Harris and M. H. Ebinger: *Soil Sci. Soc. Am. J.*, **74** (2010), 87. https://doi.org/10.2136/sssaj2009.0102
30) F. J. Wallis, B. L. Chadwick and R. J. S. Morrison: *Appl. Spectrosc.*, **54** (2000), 1231. https://doi.org/10.1366/0003702001950814
31) V. N. Vapnik: Statistical Learning Theory, JohnWiley & Sons, Inc., New York, (1998), 1.
32) C. Eum, D. Jang, J. Kim, S. Choi, K. Cha and H. Chung: *Spectrochim. Acta B*, **149** (2018), 281. https://doi.org/10.1016/j.sab.2018.09.004
33) C. P. Lu, G. Lv, C. Y. Shi, D. Y. Qiu, F. X. Jin, M. Gu and W. Sha: *Appl. Opt.*, **59** (2020), 8582. https://doi.org/10.1364/AO.401405
34) T. F. Boucher, M. V. Ozanne, M. L. Carmosino, M. D. Dyar, S. Mahadevan, E. A. Breves, K. H. Lepore and S. M. Clegg: *Spectrochim. Acta B*, **107** (2015), 1. https://doi.org/10.1016/j.sab.2015.02.003
35) Q. Shi, G. H. Niu, Q. Y. Lin, T. Xu, F. J. Li and Y. X. Duan: *J. Anal. At. Spectrom.*, **30** (2015), 2384. https://doi.org/10.1039/C5JA00255A
36) H. D. Li, Y. Z. Liang and Q. S. Xu: *Chemom. Intell. Lab. Syst.*, **95** (2009), 188. https://doi.org/10.1016/j.chemolab.2008.10.007
37) C. C. Chang and C. J. Lin: LIBSVM -- A Library for Support Vector Machines, https://www.csie.ntu.edu.tw/~cjlin/libsvm/index.html, (accessed 2021-06-10).
38) S. C. Yao, Y. L. Shen, K. J. Yin, G. Pan and J. D. Lu: *Energy Fuels*, **29** (2015), 1257. https://doi.org/10.1021/ef502174q
39) A. W. Miziolek, V. Palleschi and I. Schechter, eds.: Laser Induced Breakdown Spectroscopy (LIBS), Fundamentals and Applications, Cambridge University Press, Cambridge, UK, (2006), 1.
40) Z. Wang, M. S. Afgan, W. Gu, Y. Z. Song, Y. Wang, Z. Y. Hou, W. R. Song and Z. Li: *TrAC Trends Anal. Chem.*, **143** (2021), 116385. https://doi.org/10.1016/j.trac.2021.116385